SCIENCE CHINA
Technological Sciences

July 2010 Vol.53 No.7: 1774–1784
doi: 10.1007/s11431-010-4027-z

An effective and practical method for solving an unnegligible problem inherent in the current calculation model for multi-support seismic analysis of structures

LIU GuoHuan[2], GUO Wei[1*] & LI HongNan[2]

[1] *National Engineering Laboratory for High Speed Railway Construction, School of Civil Engineering and Architecture, Central South University, Changsha 410075, China;*
[2] *Faculty of Infrastructure Engineering, Dalian University of Technology, Dalian 116024, China*

Received April 12, 2010; accepted May 24, 2010

In the seismic analysis of extended structures subject to spatially varying motions, the displacement input model instead of acceleration model is usually adopted for accurate results. In this paper, a more detailed and comprehensive analysis of the displacement input model is carried out and the research shows that there exists an unnegligible problem in the current displacement model, which leads to the irrationality and unconvergence of some calculated results such as base shear etc. Based on the situation, an effective method named massless rigid element (MRE) method is presented to solve the problem. Moreover, the rationality and accuracy of the method are further assessed and the method is applied to a transmission tower-line system project using the commercially available structural analysis software SAP2000. The theoretical and numerical analyses indicate that the MRE approach is not only feasible with sufficient computational accuracy but also practical and can be easily implemented using the commercially available finite element software such as SAP2000.

extended structures, seismic responses, spatially varying motions, displacement input model, massless rigid element (MRE), transmission tower-line system

Citation: Liu G H, Guo W, Li H N. An effective and practical method for solving an unnegligible problem inherent in the current calculation model for multi-support seismic analysis of structures. Sci China Tech Sci, 2010, 53: 1774–1784, doi: 10.1007/s11431-010-4027-z

1 Introduction

As it is well known, most structural seismic analyses are usually based on the relative-response formulation named uniform acceleration input model, which is based on the uniform base acceleration time history input. The uniform acceleration input model is extensively adopted in the structural seismic analysis by researchers and the structural responses (i.e. displacement, velocity and acceleration) relative to ground can be directly obtained. However, according to the actual conditions, the earthquake ground motion is usually characterized by variations in time and space (i.e. the wave passage effect, site coherence effect and local site effect) and the differences in the support motions have significant influence on the structural internal forces [1, 2], especially in the extended structure such as long-span bridge, transmission tower-line system and underground tunnel. Thus, in the case of multi-support seismic excitations, structural responses are usually calculated by adopting the absolute-response formulation named displacement input model. The displacement input model is not only suitable to the case of uniform ground motion input but also multi-support input, so it is generally regarded as a universal model for the seismic response analysis. Based on the displacement input model, time history responses of the

*Corresponding author (email: wei.guo.86@gmail.com)

structure were systematically studied by Yamamura, Hao, Su and Kahan [3–8] and the response spectrum method for the seismic analysis was further studied and developed by Armen Der, Berrah, Li and Ye [2, 9–14].

In this paper, a detailed and comprehensive analysis of the displacement input model is conducted and it is explicitly pointed out that there exists an unnegligible problem in the current model, which will lead to the irrational and unconvergent calculation result (i.e. base shear). Furthermore, it would lead to incorrect structural design despite the reasonable fine-mesh finite element model. In order to solve the problem, the paper presents an effective and practical method, the massless rigid element (MRE), which is established and explained from the perspective of physics. Finally, a simple numerical example is given to verify the feasibility and accuracy of the method, and a transmission tower-line system is also analyzed by using the commercially available computer software SAP2000 to further verify the practicability of this method. Considering that the commercially available finite element programs usually have integrated the current displacement input model, the significant advantage of the MRE method is that it can be directly adopted and implemented in available finite element program without modifying the software routine.

2 Theoretical analysis of current displacement inout model

In this section, the detailed numerical research shows that there exists an unnegligible problem inherent in the current model and it would directly lead to irrational and unconvergent calculation results.

2.1 Review of current displacement input model

The equations of motion for a discretized, *n*-degree-of-freedom structural system (Figure 1) subjected to *m* support motions can be expressed in the following matrix form

$$\begin{bmatrix} \boldsymbol{M}_{nn} & \boldsymbol{M}_{ns} \\ \boldsymbol{M}_{ns}^{\mathrm{T}} & \boldsymbol{M}_{ss} \end{bmatrix} \begin{Bmatrix} \ddot{\boldsymbol{X}}_t \\ \ddot{\boldsymbol{U}}_s \end{Bmatrix} + \begin{bmatrix} \boldsymbol{C}_{nn} & \boldsymbol{C}_{ns} \\ \boldsymbol{C}_{ns}^{\mathrm{T}} & \boldsymbol{C}_{ss} \end{bmatrix} \begin{Bmatrix} \dot{\boldsymbol{X}}_t \\ \dot{\boldsymbol{U}}_s \end{Bmatrix} + \begin{bmatrix} \boldsymbol{K}_{nn} & \boldsymbol{K}_{ns} \\ \boldsymbol{K}_{ns}^{\mathrm{T}} & \boldsymbol{K}_{ss} \end{bmatrix} \begin{Bmatrix} \boldsymbol{X}_t \\ \boldsymbol{U}_s \end{Bmatrix} = \begin{Bmatrix} 0 \\ \boldsymbol{R}_m \end{Bmatrix}, \tag{1}$$

where $\boldsymbol{X}_t = [x_1(t), \cdots, x_i(t), \cdots, x_n(t)]$ is the *n*-vector of all the unknown nodal displacements at the unconstrained degrees of freedom; $\boldsymbol{U}_s = [u_1(t), \cdots, u_j(t), \cdots, u_m(t)]$ is the *m*-vector of all the known nodal displacements at the support degrees of freedom; $\boldsymbol{M}_{nn}$, $\boldsymbol{C}_{nn}$ and $\boldsymbol{K}_{nn}$ are the $n \times n$ mass, damping and stiffness matrices associated with the unconstrained degrees of freedom, respectively; $\boldsymbol{M}_{ss}$, $\boldsymbol{C}_{ss}$ and $\boldsymbol{K}_{ss}$ are the $m \times m$ matrices associated with the support degrees of freedom; $\boldsymbol{M}_{ns}$, $\boldsymbol{C}_{ns}$ and $\boldsymbol{K}_{ns}$ are the $n \times m$ coupled matrices associated with the both sets of degrees of freedom and $\boldsymbol{R}_m$ is the *m*-vector of reacting forces at the support degrees of freedom. For a lumped-mass system, $\boldsymbol{M}_{ns}$=0.

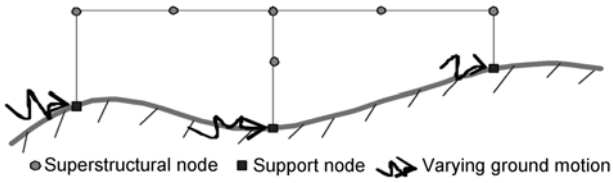

Figure 1 Sketch of structure subjected to multi-support ground motions.

From eq. (1), the equilibrium equations for the superstructure can be written as

$$\boldsymbol{M}_{nn}\ddot{\boldsymbol{X}}_t + \boldsymbol{C}_{nn}\dot{\boldsymbol{X}}_t + \boldsymbol{K}_{nn}\boldsymbol{X}_t = -\boldsymbol{K}_{ns}\boldsymbol{U}_s - \boldsymbol{C}_{ns}\dot{\boldsymbol{U}}_s. \tag{2}$$

Generally, the damping matrix $\boldsymbol{C}_{ns}$ is not defined [15]. Therefore, the damping forces $-\boldsymbol{C}_{ns}\dot{\boldsymbol{X}}_s$ are normally neglected and eq. (2) can be rewritten in the following form:

$$\boldsymbol{M}_{nn}\ddot{\boldsymbol{X}}_t + \boldsymbol{C}_{nn}\dot{\boldsymbol{X}}_t + \boldsymbol{K}_{nn}\boldsymbol{X}_t = -\boldsymbol{K}_{ns}\boldsymbol{U}_s. \tag{3}$$

Eq. (3) is named as the displacement input model since the displacement time histories $\boldsymbol{U}_s$ is used as input [15, 16]. As it is well known, the displacement input model is usually used for calculating the seismic responses of structures, especially of those extended structures subjected to spatially varying seismic excitations.

2.2 Transformation of displacement input model

In order to clarify the real meaning of the displacement input model, the formulation of displacementinput model is transformed and a further comprehensive study is carried out in this section. Thus, $\boldsymbol{X}_t$ can be expressed as follows:

$$\boldsymbol{X}_t = \boldsymbol{X}_t^p + \boldsymbol{X}_t^d, \tag{4}$$

where $\boldsymbol{X}_t^p$ and $\boldsymbol{X}_t^d$ refer to the pseudo-static and dynamic displacements, respectively.

It is important to note that eq. (4) is a geometric equation and is not restricted to linear problems and it is not consistent with the previous attitude [15]. This reason is that $\boldsymbol{X}_t^p$ and $\boldsymbol{X}_t^d$ are the two parts of $\boldsymbol{X}_t$ instead of two kinds of responses generated respectively by different excitations. When the inertial effect is not considered (at this time, the damping force $\boldsymbol{C}_{nn}\dot{\boldsymbol{X}}_t$ and dynamic displacement $\boldsymbol{X}_t^d$ do not exist), the equations for the superstructural nodes from eq. (1) can be written as follows:

$$\boldsymbol{K}_{nn}\boldsymbol{X}_t^p + \boldsymbol{K}_{ns}\boldsymbol{U}_s = 0 \Rightarrow \boldsymbol{X}_t^p = -\boldsymbol{K}_{nn}^{-1}\boldsymbol{K}_{ns}\boldsymbol{U}_s. \tag{5}$$

Here, the classical Rayleigh damping matrix is expressed as

$$\boldsymbol{C}_{nn} = \eta\boldsymbol{M}_{nn} + \zeta\boldsymbol{K}_{nn}, \tag{6}$$

where η and ζ denote the mass-proportional and stiffness-proportional damping coefficients, respectively. They can be obtained from the following formulation:

$$\begin{Bmatrix}\eta\\ \zeta\end{Bmatrix}=\frac{2\xi}{\omega_m+\omega_n}\begin{Bmatrix}\omega_m\omega_n\\ 1\end{Bmatrix}, \tag{7}$$

where ω_m and ω_n are the circular frequencies of the mth and nth modes, respectively, ξ is the modal damping ratio and usually is set to a value between 2% and 5%.

Substituting eqs. (4), (5) and (6) into eq. (3) yields the following dynamic equilibrium equations in terms of dynamic responses $\boldsymbol{X}_t^d$, $\dot{\boldsymbol{X}}_t^d$ and $\ddot{\boldsymbol{X}}_t^d$ of the superstructure:

$$\begin{aligned}&\boldsymbol{M}_{nn}\ddot{\boldsymbol{X}}_t^d+\boldsymbol{C}_{nn}\dot{\boldsymbol{X}}_t^d+\boldsymbol{K}_{nn}\boldsymbol{X}_t^d\\&=-\boldsymbol{M}_{nn}\boldsymbol{K}_{nn}^{-1}\boldsymbol{K}_{ns}\ddot{\boldsymbol{U}}_s-\eta\boldsymbol{M}_{nn}\boldsymbol{K}_{nn}^{-1}\boldsymbol{K}_{ns}\dot{\boldsymbol{U}}_s+\zeta\boldsymbol{K}_{ns}\dot{\boldsymbol{U}}_s.\end{aligned} \tag{8}$$

From the analysis above, it can be seen that eq. (3) is equivalent to eq. (8) in the mathematical meaning. In other words, when eq. (8) is used to calculate the structural seismic responses of the actual physical model subjected to non-uniform earthquake ground motions as illustrated in Figure 2, the structural dynamic responses obtained from eq. (3) are equal to those calculated from eq. (8), whose physical model can be correspondingly illustrated by Figure 3. In Figure 3, it can be noticed that the vector $\zeta\boldsymbol{K}_{ns}\dot{\boldsymbol{U}}_s$ is the nodal forces only acting on the joints adjacent to the support nodes.

2.3 Comprehensive analysis of displacement input model

Firstly, only the uniform earthquake ground motion is considered here as a simple situation. In the case of uniform earthquake excitation, it is apparent that $\boldsymbol{X}_t^p$ can be directly written as

$$\boldsymbol{X}_t^p=\boldsymbol{E}u_g, \tag{9}$$

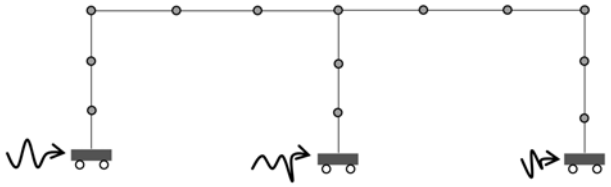

Figure 2 Sketch of an actual physical model.

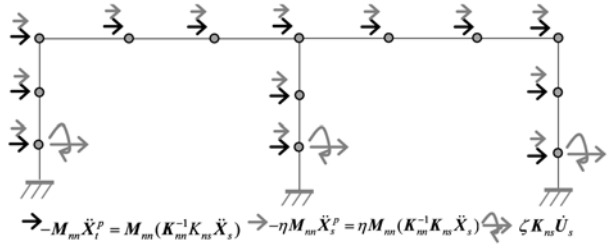

Figure 3 Sketch of the physical model corresponding to eq. (8).

where $\boldsymbol{E}$ denotes the $n\times1$ column vector with unit elements; u_g is the displacement history of the uniform earthquake ground motion. Then, it follows that

$$\eta\boldsymbol{M}_{nn}\boldsymbol{K}_{nn}^{-1}\boldsymbol{K}_{ns}\dot{\boldsymbol{U}}_s=\eta\boldsymbol{M}_{nn}\boldsymbol{E}\dot{u}_g,\ \ \zeta\boldsymbol{K}_{ns}\dot{\boldsymbol{U}}_s=\zeta\boldsymbol{K}_{ns}\dot{u}_g. \tag{10}$$

In this case, eq. (8) can be further rewritten as

$$\begin{aligned}&(\boldsymbol{M}_{nn}\ddot{\boldsymbol{X}}_t^d+\boldsymbol{C}_{nn}\dot{\boldsymbol{X}}_t^d+\boldsymbol{K}_{nn}\boldsymbol{X}_t^d)/\Omega\\&=-\boldsymbol{M}_{nn}\boldsymbol{E}\ddot{u}_g-\eta\boldsymbol{M}_{nn}\boldsymbol{E}\dot{u}_g-\zeta\boldsymbol{K}_{ns}\dot{u}_g.\end{aligned} \tag{11}$$

It is known that the Ω in eq. (11) is just the uniform acceleration input model for calculating structural seismic responses. This model is very familiar to the researcher engaged in seismic analysis and its physical model can be illustrated by Figure 4. Therefore, compared with the correct acceleration model Ω, two more loads are applied on the structure in eq. (11) which is the transformation form of displacement inpute model, so it would lead to indirect results in some situations.

Secondly, there are two questions that we may be interested in: a) How do $\eta\boldsymbol{M}_{nn}\boldsymbol{E}\dot{u}_g$ ($\eta\boldsymbol{M}_{nn}\boldsymbol{K}_{nn}^{-1}\boldsymbol{K}_{ns}\dot{\boldsymbol{U}}_s$) and $\zeta\boldsymbol{K}_{ns}\dot{u}_g$ ($\zeta\boldsymbol{K}_{ns}\dot{\boldsymbol{U}}_s$) act on the structure, respectively? b) In contrast with $-\boldsymbol{M}_{nn}\boldsymbol{E}\ddot{u}_g$ ($-\boldsymbol{M}_{nn}\boldsymbol{K}_{nn}^{-1}\boldsymbol{K}_{ns}\ddot{\boldsymbol{U}}_s$), can the influence of the two terms on the structural responses be ignored?

For convenience, the case of uniform earthquake input is discussed below.

1) Evaluation of $\eta\boldsymbol{M}_{nn}\boldsymbol{E}\dot{u}_g$: From Figure 3, it is apparent to realize that the physical meaning of the vector $\eta\boldsymbol{M}_{nn}\boldsymbol{E}\dot{u}_g$ denotes the concentrated forces acting on each lumped-mass point of the superstructure. In contras with the jth component of the vector $-\boldsymbol{M}_{nn}\boldsymbol{E}\ddot{u}_g$, the influence of that of $\eta\boldsymbol{M}_{nn}\boldsymbol{E}\dot{u}_g$ on the structural responses can be evaluated by the following expression:

$$\delta_j=\frac{\sigma\left\{\eta\boldsymbol{M}_{nn}\boldsymbol{E}\dot{u}_g\right\}_j}{\sigma\left\{\boldsymbol{M}_{nn}\boldsymbol{E}\ddot{u}_g\right\}_j}=\eta\frac{\sigma_{\dot{u}_g}}{\sigma_{\ddot{u}_g}}=\eta\cdot\kappa,\quad(j=1,2,\cdots,m), \tag{12}$$

where $\{\}_j$ represents the jth component of the vector $\{\}$.

The term δ_j is to be discussed from a statistical perspective on the assumption that u_g is a stationary and zero-mean

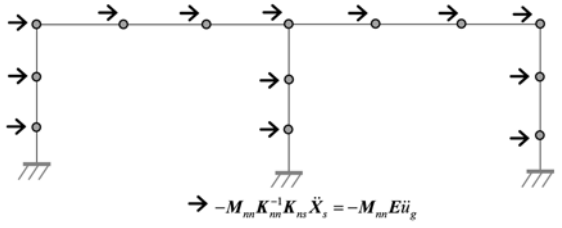

Figure 4 Sketch of physical model corresponding to uniform acceleration input model.

random process. Then, based on the random vibration theory, κ can be written as

$$\kappa = \frac{\sigma_{\dot{u}_g}}{\sigma_{\ddot{u}_g}} = \frac{\int_0^{+\infty} S_{\dot{u}_g}(\omega)\mathrm{d}\omega}{\int_0^{+\infty} S_{\ddot{u}_g}(\omega)\mathrm{d}\omega} = \frac{\int_0^{+\infty} [\frac{1}{\omega^2} S(\omega)]\mathrm{d}\omega}{\int_0^{+\infty} S(\omega)\mathrm{d}\omega}, \quad (13)$$

where $S(\omega)$ is the unilateral power spectral density function of $\ddot{u}_g$.

Generally, the following expressions are rational and can be directly given in response to the characteristics of earthquake ground motions:

$$T_p < 1.0\ s, \quad (14)$$

or

$$\omega_p > \frac{2\pi}{T_p} = 2\pi \cong 6.28\ \text{rad/s}, \quad (15)$$

where T_p and ω_p represent the predominant period and circular frequency of earthquake ground acceleration history, respectively. In other words, the major energy of $\ddot{u}_j(t)$ focuses on the vicinity of ω_p and then eq. (13) can be approximately written as follows:

$$\kappa = \frac{\sigma_{\dot{u}_g}}{\sigma_{\ddot{u}_g}} \cong \frac{\int_{\omega_p-\Delta}^{\omega_p+\Delta} [\frac{1}{\omega^2} S_j(\omega)]\mathrm{d}\omega}{\int_{\omega_p-\Delta}^{\omega_p+\Delta} S_j(\omega)\mathrm{d}\omega}, \quad (16)$$

where Δ denotes the interval in the vicinity of ω_p. In the range of $[\omega_p-\Delta, \omega_p+\Delta]$, it is apparent that $S_j(\omega)/\omega^2$, compared with $S_j(\omega)$, is very small so that $\int_{\omega_p-\Delta}^{\omega_p+\Delta}\left[\frac{1}{\omega^2} S_j(\omega)\right]\mathrm{d}\omega$ can be ignored in contrast with $\int_{\omega_p-\Delta}^{\omega_p+\Delta} S_j(\omega)\mathrm{d}\omega$ because the value of ω_p is no less than $2\pi s$. In another word, the term κ is small enough to be ignored. Moreover, for a normal structure without considerable rigidity as well as with ξ that ranges from 2%–5%, the value of η computed from eq. (7) is also small. Subsequently, it is concluded that the value of σ_{δ_j} is small or that the influence of $\alpha \boldsymbol{M}_{nn}\boldsymbol{K}_{nn}^{-1}\boldsymbol{K}_{ns}\ddot{\boldsymbol{U}}_s$ on the structural responses can be ignored.

2) Evaluation of $\zeta \boldsymbol{K}_{ns}\dot{\boldsymbol{U}}_s$: As shown in Figure 3, the physical meaning of the vector $\zeta \boldsymbol{K}_{ns}\dot{\boldsymbol{U}}_s$ is the nodal forces only acting on the joints adjacent to the support nodes; the stiffnessmatrix $\boldsymbol{K}_{ns}$ only has terms associated with the joints adjacent to the base nodes where the displacement histories are applied and the magnitude of non-zero elements in the matrix element of $\boldsymbol{K}_{ns}$ is the stiffness of the bottom elements. It is known that according to the finite element method, the magnitude of the bottom element stiffness is directly dependent on the element division and the magnitude of matrix elements of $\boldsymbol{K}_{ns}(j)$ increases with the bottom element refinement. For a sufficiently fine-meshed model, the value of ζ by eq. (7) is determined, in spite of a more refined model, as soon as m, n and ξ are definitely selected. However, the more refined bottom element division will make the value of matrix elements of $\boldsymbol{K}_{ns}(j)$ increase and undoubtly cause an increase of matrix elements of $\zeta \boldsymbol{K}_{ns}\dot{\boldsymbol{U}}_s$, which will directly lead to the increasement of the bottom element internal forces. As a matter of fact, for a sufficiently fine-meshed model, the structural responses are definite and convergent instead of continuously alternating with the refinement of model. Thus, unlike $\eta \boldsymbol{M}_{nn}\boldsymbol{K}_{nn}^{-1}\boldsymbol{K}_{ns}\dot{\boldsymbol{U}}_s$, the influence of $\zeta \boldsymbol{K}_{ns}\dot{\boldsymbol{U}}_s$ on the structural responses is unnegligible. Thus, the displacement input model could lead to indirect results in the seismic analysis because of the unnegligible extra load $\zeta \boldsymbol{K}_{ns}\dot{\boldsymbol{U}}_s$ on the structure. From the above analysis, Figure 3 can be approximately illustrated in Figure 5.

2.4 Further numerical investigation

In this section, the error induced by the current displacemeng model will be proved in the numerical simulation. Moreover, in order to adequately verify the theoretical analysis in sections 2.2 and 2.3, $\eta \boldsymbol{M}_{nn}\boldsymbol{K}_{nn}^{-1}\boldsymbol{K}_{ns}\dot{\boldsymbol{U}}_s$ and $\zeta \boldsymbol{K}_{ns}\dot{\boldsymbol{U}}_s$ are also needed to be considered individually. In this section, a structure as shown in Figure 5 is taken as an example for further verification, and the uniform earthquake excitation is adopted firstly for numerical simulation.

In Figure 6, E, ρ, I and A denote the elastic modulus, material density, inertial moment and cross-sectional area, respectively; B, C, S and E represent the beam, column, support node and bottom element of each column, respectively. The local in-plane stiffness matrix for beam elements, $\boldsymbol{k}^e$, is selected as

$$\boldsymbol{k}^e = \begin{bmatrix} EA/l & 0 & 0 & -EA/l & 0 & 0 \\ & 12EI/l^3 & 6EI/l^2 & 0 & -12EI/l^3 & 6EI/l^2 \\ & & 4EI/l & 0 & -6EI/l^2 & 2EI/l \\ & & & EA/l & 0 & 0 \\ & \text{Sym} & & & 12EI/l^3 & -6EI/l^2 \\ & & & & & 4EI/l \end{bmatrix}. \quad (17)$$

To give adequate verification, three kinds of cases are

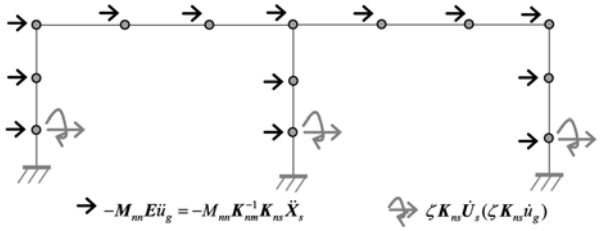

Figure 5 Sketch of approximate physical model corresponding to eq. (8).

investigated. The natural vibration periods of the structure for different cases are shown in Table 1, in which N_b and N_c are equal division numbers of each beam and each column, respectively. It can be deduced from Table 1 that the sufficient computational accuracy can be obtained through the analysis of case 1 (Nc=16). The first several mode shapes of the structure are illustrated in Figure 7.

1) The time history responses of the structures subjected to E_1 Centro 1940 NS ground motion are investigated as shown in Figure 8. The Hilbert–Huang Taylor direct integration method [17] is used to calculate the structural dynamic responses and the specific integration parameters are γ=0.5, β=0.25 and α=0.

2) Evaluation of $\eta \boldsymbol{M}_{nn}\boldsymbol{K}_{nn}^{-1}\boldsymbol{K}_{ns}\dot{\boldsymbol{U}}_s$.

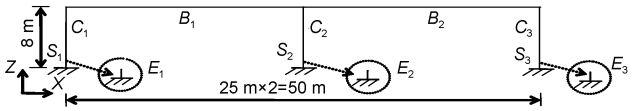

Figure 6 Numerical example. E=2.48×10^{10} Pa, ρ=2400 kg/m^3, I_{B1}= I_{B2}= 8.64×10^{-2} m^4, I_{c1}= I_{c2}= I_{c3}=1.08×10^{-2} m^4, A_{B1}=A_{B2}=7.2×10^{-1} m^2, A_{C1}= A_{C2}= A_{C3}=3.6×10^{-1} m^2.

Table 1 Vibration characteristics of different meshed models

Case	1	2	3
N_b		50	
N_c	16	32	64
ω_1 (rad/s)	13.28	13.28	13.28
ω_2 (rad/s)	15.40	15.40	15.40
η/ξ	0.57/0.28×10^{-2}	0.57/0.28×10^{-2}	0.57/0.28×10^{-2}

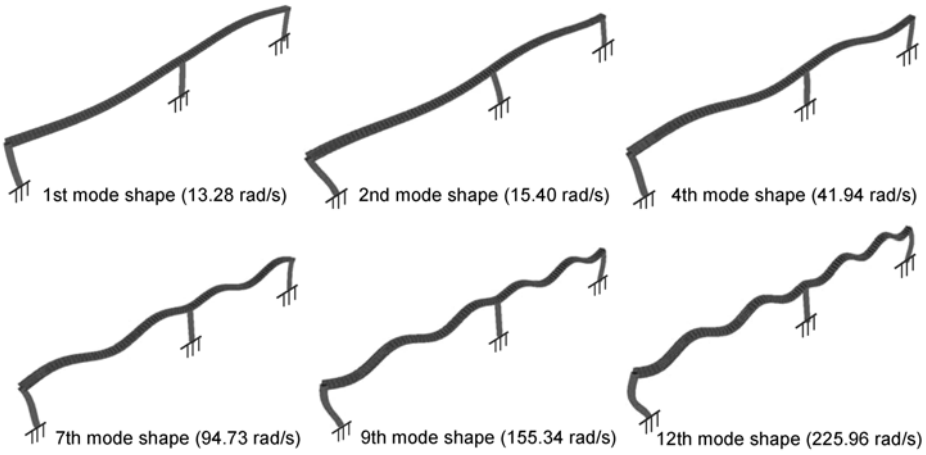

Figure 7 Mode shapes of structure.

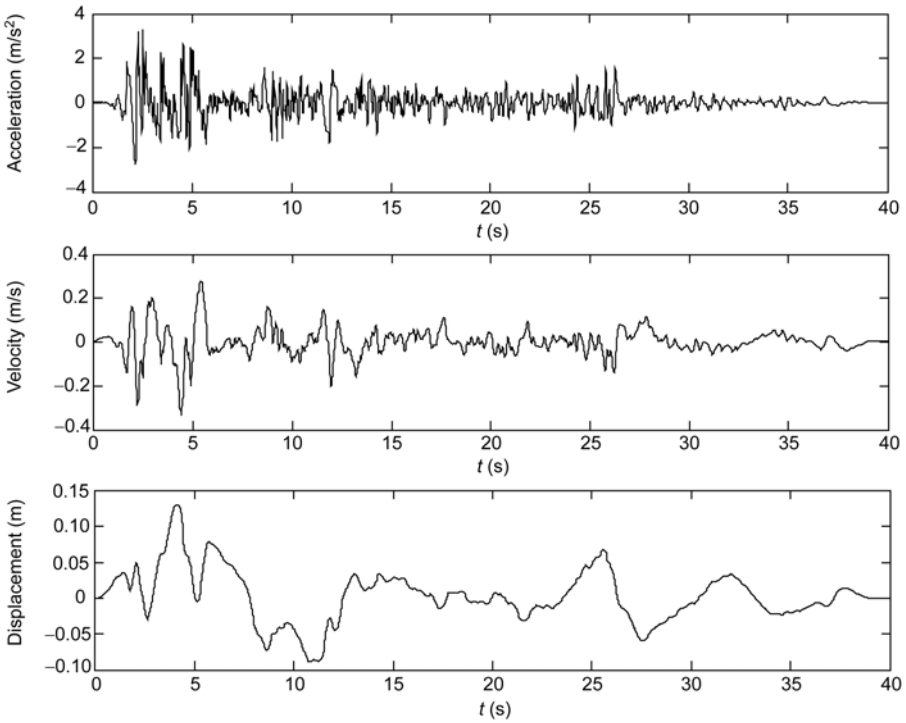

Figure 8 E_1 Centro time history curves (1940 NS).

The shear force of each bottom element for case 1 (Nc= 16) is shown in Figure 9 and the maximum values of shear forces are compared and given in Table 2. From Table 2, it can be seen that the maximum error between cases a (η=ζ=0) and b (η=0.57, ζ=0) is 7.4409%, which further indicates that the the influence of $\alpha \boldsymbol{M}_{nn}\boldsymbol{K}_{nn}^{-1}\boldsymbol{K}_{ns}\ddot{\boldsymbol{U}}_s$ on the structural responses can be ignored. Through the theretical analysis, it is noted that conservative results calculated from case b, compared with those from a, can be obtained due to the existence of $\alpha \boldsymbol{M}_{nn}\boldsymbol{K}_{nn}^{-1}\boldsymbol{K}_{ns}\ddot{\boldsymbol{U}}_s$.

3) Evaluation of $\zeta \boldsymbol{K}_{ns}\dot{\boldsymbol{U}}_s$.

The shear forces of each bottom element for different cases are also obtained and the calculational results are given in Figure 10. It can be shown that the bottom shear forces increase with the increase of element division number and exhibit a nonconvergent tendency. As a matter of fact, however, the structural internal forces should be deterministic if the structure and earthquake motion are known. The results further verifies the theoretical analysis of the influence of $\zeta \boldsymbol{K}_{ns}\dot{\boldsymbol{U}}_s$ discussed above.

3 Massless rigid element(MRE) method for unnegligibale problem

In this section, an effective practical method called MRE is presented to solve the unnegligible problem induced by $\zeta \boldsymbol{K}_{ns}\dot{\boldsymbol{U}}_s$.

Table 2 Comparision of maximum shear force values of bottom elements

Comparision cases	Maximum shear force value of each bottom element (10^5×N)		
	E_1	E_2	E_3
a : η=ζ=0	2.0022	2.1735	2.0022
b: η=0.57, ζ= 0	2.0423	2.3352	2.0423
[(a–b)/a]×100%	–2.0051%	–7.4409%	–2.0051%

3.1 Presentation of MRE method

According to the analysis in the previous section, the physical meaning of $\zeta \boldsymbol{K}_{ns}\dot{\boldsymbol{U}}_s$ is the concentrated forces which only act on the nodes adjacent to the support joints. In such a case, it is easily considered that adding elements to the support joints of structure can implement a shift of the action points of $\zeta \boldsymbol{K}_{ns}\dot{\boldsymbol{U}}_s$ from j to j_1 as illustrated in Figure 11. From the figure, we can see that the original structure and the added elements constitute a new structure, in which the original structure naturally becomes a substructure of the new structure.

Here, three conditions, (a) sufficient rigidity, (b) masslessness, and (c) counterforce $\zeta \boldsymbol{K}_{ns}\dot{\boldsymbol{U}}_s$, are assigned to the

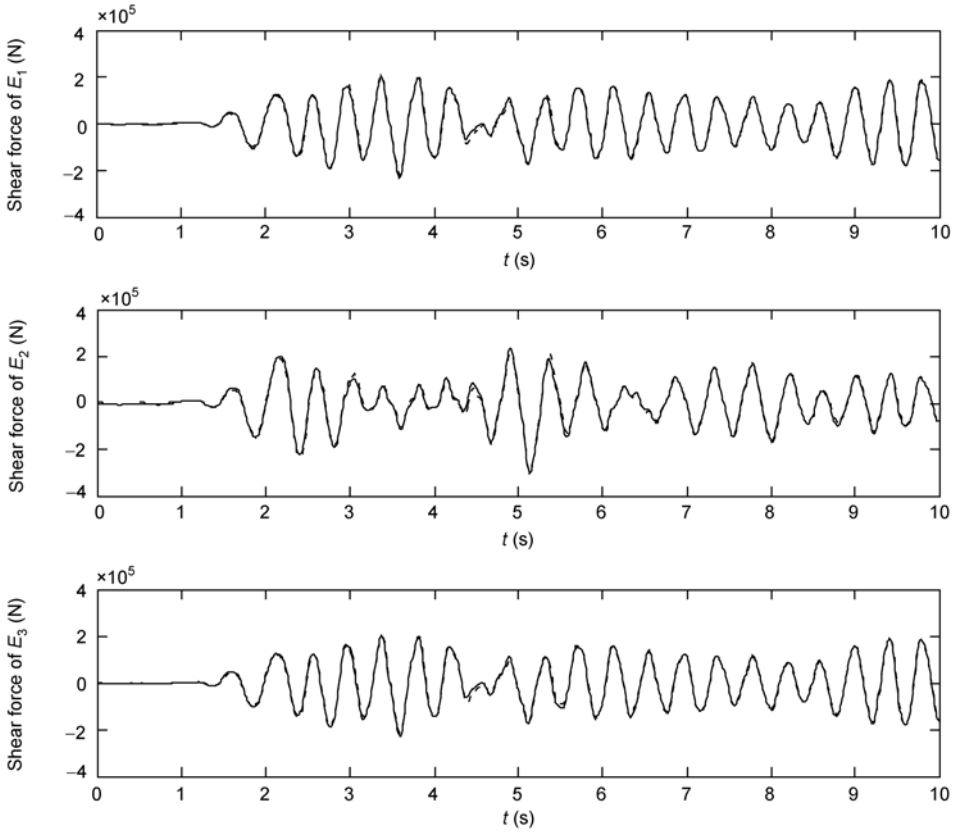

Figure 9 Shear force histories of bottom element (Nc=16).

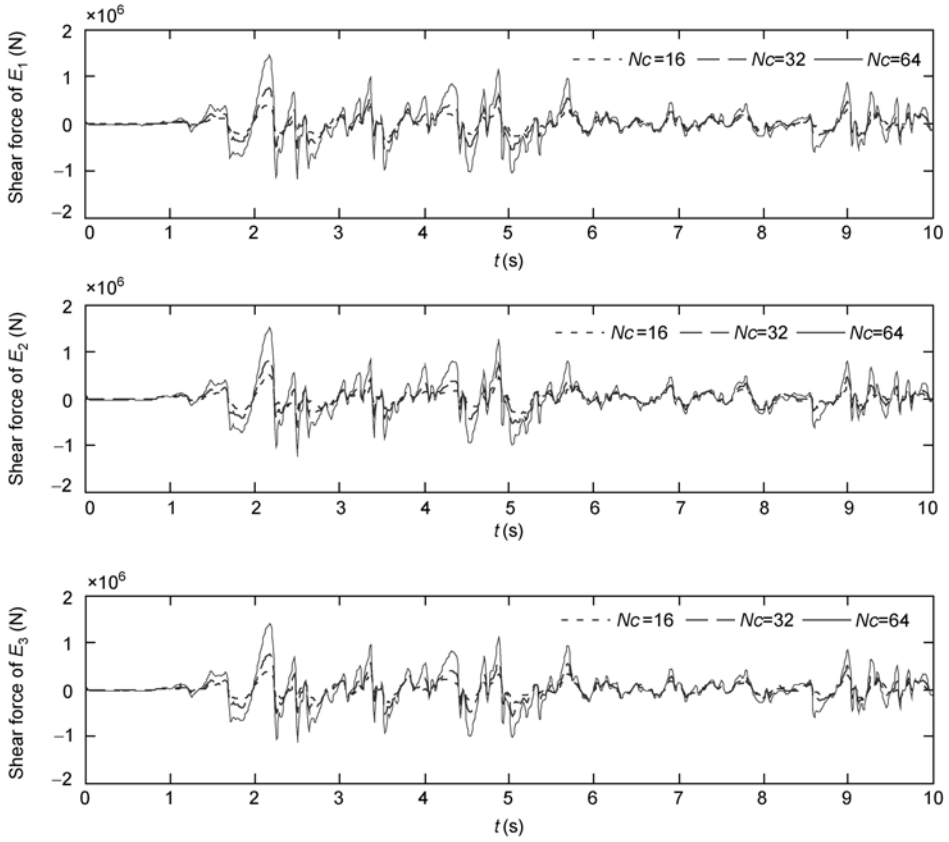

Figure 10 Shear force histories of bottom element only considering stiffness-proportional damping (η=0, ξ=0.28×10^{-2}).

added elements. Condition (a) is intended to assure that the MRE can be regarded as the rigid foundation of the substructure, and thus ensures the dynamic characteristics of the substructure will be the same as those of the original structure. Condition (b) avoids generating structural deformation induced by the the nodal force, $-m_{j_1}\ddot{u}_j$, acting on node j_1, unless $-m_{j_1}\ddot{u}_j \neq 0$ if $m_{j_1} \neq 0$. Condition (c) guarantees that the response of node j_1 is the same as the ground motion at the support node.

In theory, Condition (c) is necessary and can not be constituted by Condition (a) because $\zeta \boldsymbol{K}_{ns}\dot{\boldsymbol{U}}_s$ is directly related to $\boldsymbol{K}_{ns}$ that is just the stiffness of massless rigid elements. In other words, $\zeta \boldsymbol{K}_{ns}\dot{\boldsymbol{U}}_s$ will increase correspondingly with the increment of stiffness of massless rigid elements. Subsequently, relative displacement between nodes j_1 and s will be definitely generated by $\zeta \boldsymbol{K}_{ns}\dot{\boldsymbol{U}}_s$ if Condition (c) is not required and its magnitude is $\zeta\dot{\boldsymbol{U}}_s$. The deformed sketch of partial structure under the action of $\zeta \boldsymbol{K}_{ns}\dot{\boldsymbol{U}}_s$ is illustrated by Figure 12. However, according to the theory of structural mechanics, the relative displacement between nodes j_1 and s has no influence on the internal forces of the superstructure.

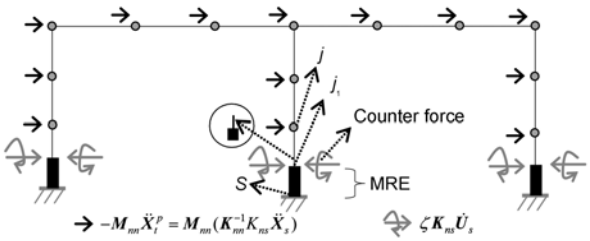

Figure 11 Sketch of the new structure.

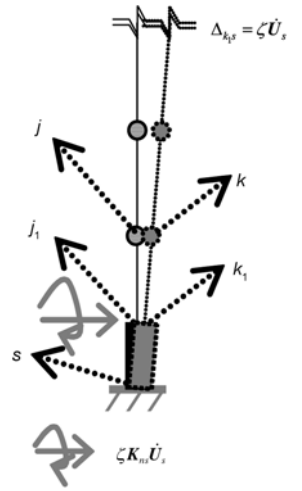

Figure 12 Deformed sketch of partial structure under action of $\zeta \boldsymbol{K}_{ns}\dot{\boldsymbol{U}}_s$.

3.2 Verification of MRE method

The purpose of this section is to conduct a further numerical verification of the MRE method presented in this paper.

To satisfy Conditions (a) and (b), the material and geometric attributes of the massless rigid element are selected and given in Table 3. In the table, W_b, H_b and L_b are respectively the width, height of cross area of the massless rigid element and the element length; E_b and ρ_b represent the material elastic modulus and density, respectively. The natural vibration characteristics of the new structure for the different cases are identical with those of the original structure, as shown in Table 1. The first several mode shapes of the new structure are illustrated in Figure 13. The fact shows that the attributes assigned to the massless rigid elements satisfy Condition (a) and the massless rigid elements can be regarded as the rigid foundation of the substructure. Certainly, other attributes that can provide enough rigidity for the massless rigid elements can also satisfy the condition.

Here, the shear force of each bottom element of substructure and displacement histories at nodes j_1 and s (Figure 14) for the three cases disscussed in Section 2.3 are reinvestigated and the calculational results are shown in Figures 15 and 16. Moreover, the maximum values of shear forces for these cases are compared and given in Table 4. From Figures 15 and 16 and Table 4, it can be seen that the shear forces are convergent and the displacement histories of nodes j_1 and s are almost identical, which further demonstrates that the efficiency and computational accuracy of the MRE method.

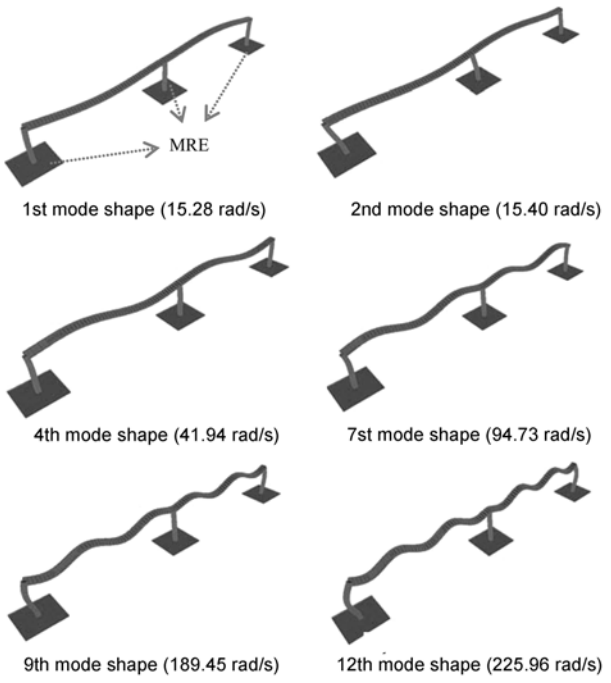

Figure 13 Mode shapes of new structure.

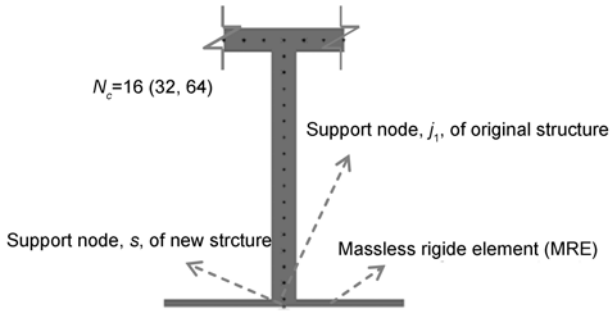

Figure 14 Sketch of support nodes of the original and new structures.

4 Application of MRE method to pratical project

In the previous section, a simple example was analyzed and the accuracy of MRE method was verified. In this section, in order to further demonstrate the practicability of the

Table 3 The material and geometric attributes of massless rigid element

Condition to be satifacted	Condition (a)			Condition (b)
Attribute	$L_b \times H_b$ (m·m)	W_b (m)	E_b (Pa)	ρ_b (kg·m^{-3})
Value	6.0×6.0	0.2	2.0×10^{11}	0

Table 4 Comparision between maximum shear force values of each bottom element

Cases and comparision	Each bottom element		
	E_1	E_2	E_3
Shear force for Case 1 (N)	192474.272	224037.389	192474.272
Shear force for Case 2 (N)	192647.696	224092.543	192647.696
Shear force for Case 3 (N)	192731.02	224108.922	192731.02
[(Case 1–Case 2)/Case 1]×100%	–0.090102%	–0.024618%	–0.090102%
[(Case 1–Case 3)/Case 1]×100%	–0.13339%	–0.031929%	–0.13339%
[(Case 2–Case 3)/Case 2]×100%	–0.043252%	–0.007309%	–0.043252%

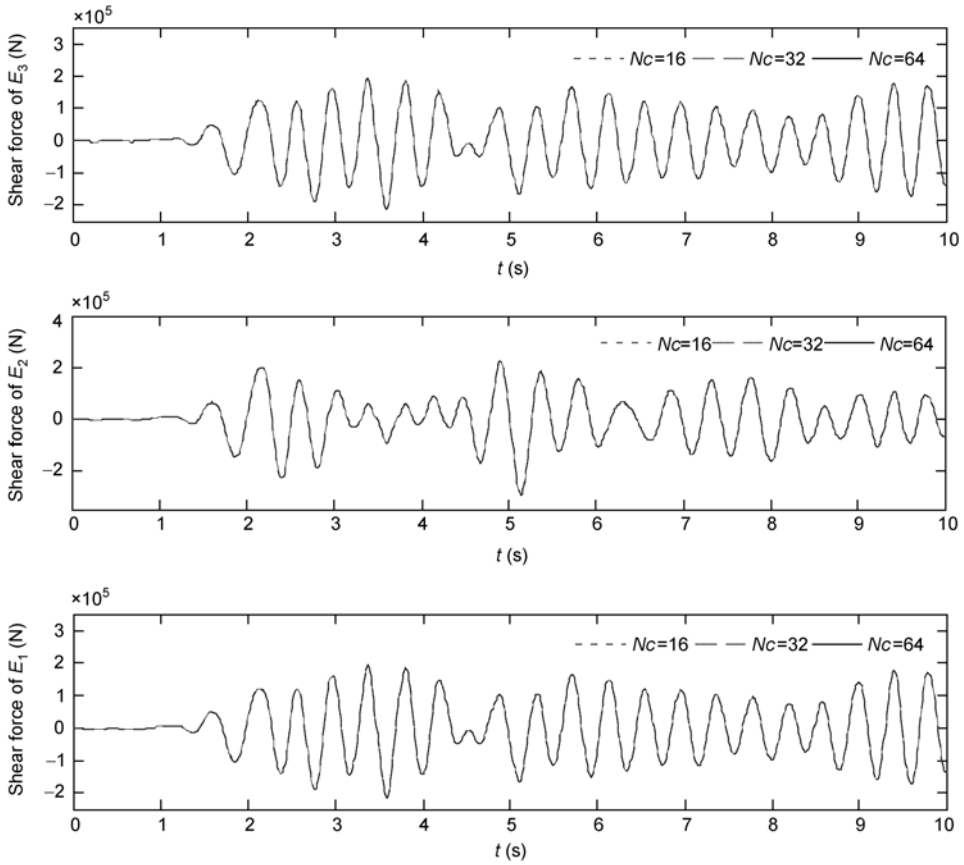

Figure 15 Comparision of shear force histories of bottom element (η=0, ξ=0.28×10^{-2}).

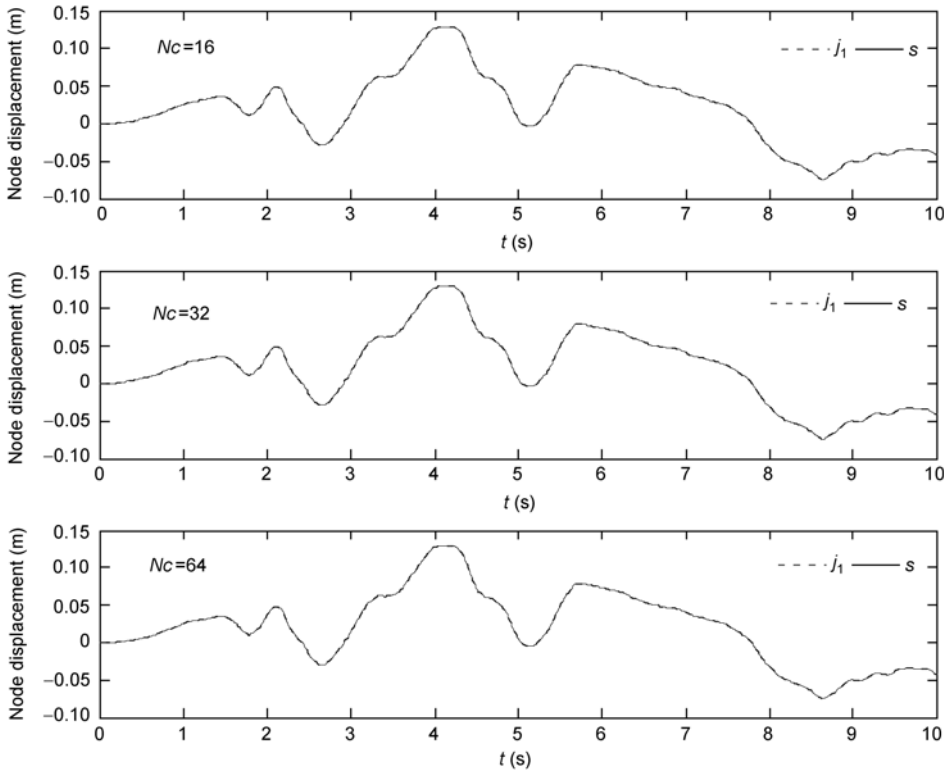

Figure 16 Comparision of node displacement histories (η=0, ξ=0.28×10^{-2}).

MRE method, the method is implemented by using finite element software SAP2000 and is applied to a transmission tower-line system project located in Gaizhou city of Liaoning Province, China.

The original and new finite element models are established as shown in Figures 17 and 18. In the new model established by MRE method, the cylinder is used to simulate the rigid element. In order to assure a sufficient rigidity of the cylinder, its cross section diameter and height are assigned to 6 m and 1 m, respectively. Comparison of the first seven-hundred natural vibration periods of the original and new structures is shown in Figure 19. From the figure, it can be seen that the natural vibration periods are almost identical, which demonstrates the stiffness of the rigid element meets the requirement. The comparison of the 1st, 298th and 625th vibration mode shapes are given in Figure 20.

Earthquake wave is selected as the previous section and the x direction is the direction of excitation. According to Condition (c) discussed in section 3.1, counterforce $\beta \boldsymbol{K}_{ts} \boldsymbol{E} \ddot{x}_g$ is applied to node S_a of new structure.

Here, the calculation results of the top-node and the bottom element illustrated in Figures 17 and 18 are investigated. Displacement time histories of nodes S_a and S_b in the new structure are given in Figure 21, from which it can be seen that they match very well. This indicates the displacement histoty of S_a is identical to the earthquake ground motion. Comparisons of displacement of the top-node and shear force of the bottom element of the original and new structures are separately given in Figures 22 and 23, which show good consistency of the calculation results. So, the MRE method can be directly implemented using finite element software and applied to practical projects.

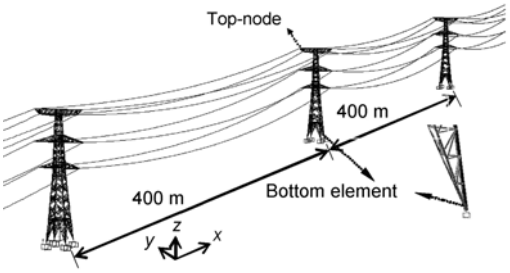

Figure 17 Finite element model of transmission tower-line system (original model).

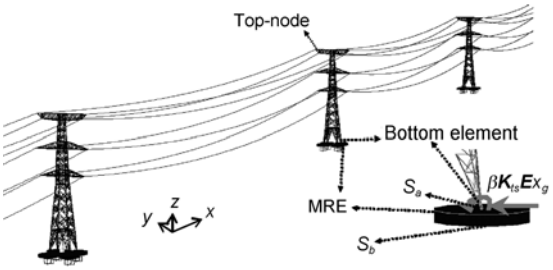

Figure 18 Finite element model of transmission tower-line system adopting MRE method (new model).

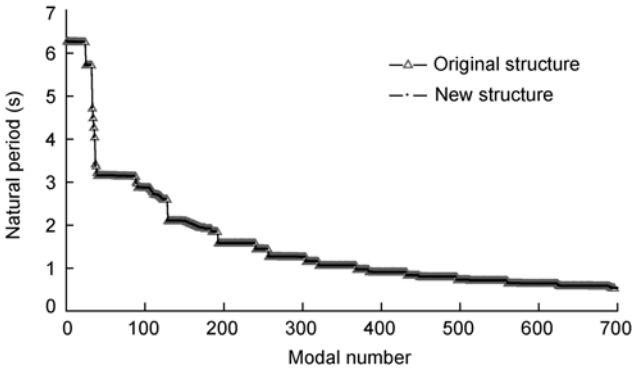

Figure 19 Comparison of the first seven-hundred natural vibration periods.

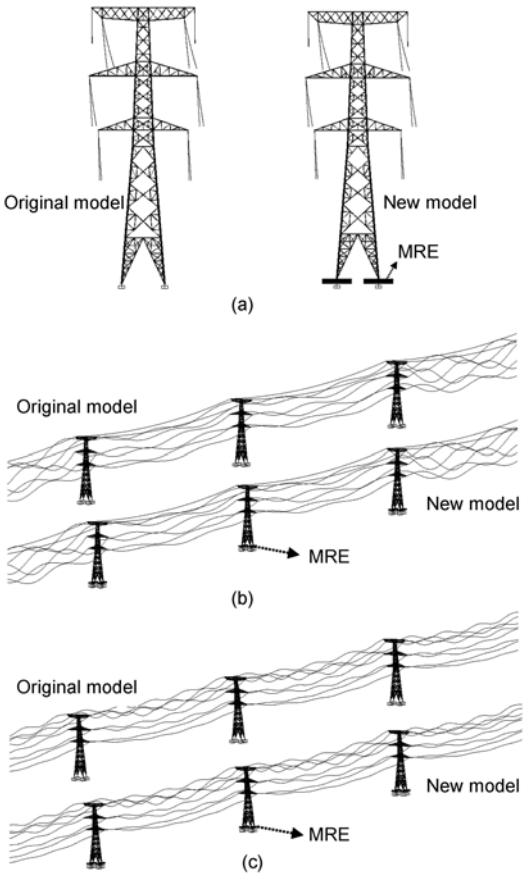

Figure 20 Comparision of mode shapes between the original and new power transmission tower line system models. (a) 1st vibration mode shape; (b) 298th vibration mode shape; (c) 625th vibration mode shape.

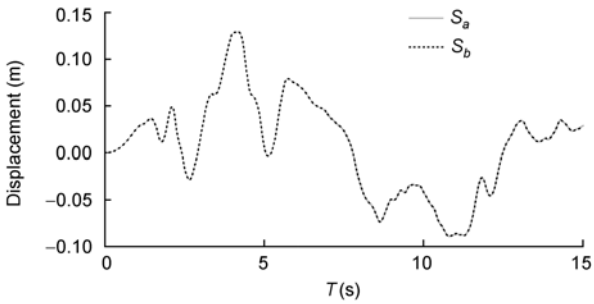

Figure 21 Comparison displacement histories of nodes S_a and S_b.

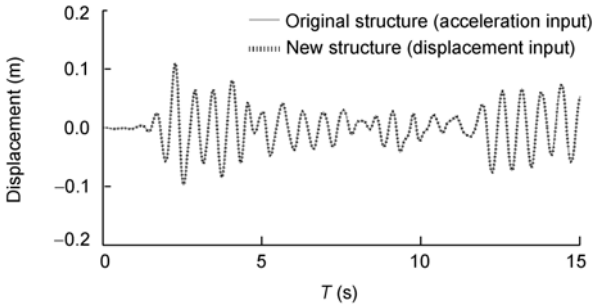

Figure 22 Comparison of top-node displacements.

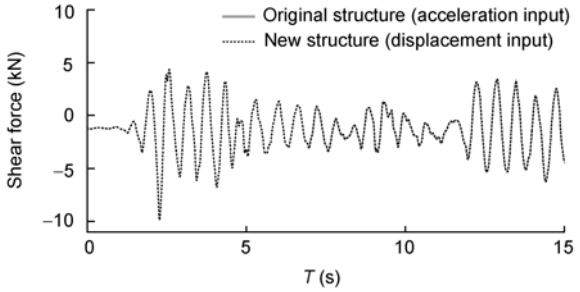

Figure 23 Comparison of bottom-element shear forces.

5 Note

It can be realized that the unnegligible problem disscussed above will not exist unless the stiffness-proportional damping is included. However, neither of the damping matrices defined by eq. (18) is appropriate for practical analysis of MOF system, because the variations of modal damping ratios with natural frequencies based on damping matrices eq. (18) are not consistent with the experimental data, which indicate roughly the same modal damping ratios for seicmic vibration [16]. Thereby, it is unreasonable to expect that the unnegligible problem inherent in the current input model "can" be solved by only assigning the mass-proportional damping matrix instead of including stiffness-proportional damping such as

$$\boldsymbol{C}_{nn} = \eta \boldsymbol{M}_{nn} \quad \text{and} \quad \boldsymbol{C}_{nn} = \zeta K_{nn}. \tag{18}$$

The criterion for assessing whether the stiffness of massless rigid element is sufficient is that the massless rigid element can be regarded as the sufficiently rigid foundations. The criterion can guarantee that the dynamic characteristics of substructure of the new structure are in essence equivalent to those of the original structure. Toward a better comprehension, the massless rigid element can be regarded as a "rigid convertor" which has the following two functions: 1) the original structure is fixed to the ground by it, 2) the concentrated forces $\zeta \boldsymbol{K}_{ns}\dot{u}_g$ acting at the original structure are shifted to the massless rigid element.

6 Conclusions

The calculation model that is widely adopted for evaluating structural seismic responses, especially for the extended structures, has been reviewed and reanalyzed in detail in this paper. The main findings and conclusions are summarized as follows.

1) It is found that there exists an unnegligible problem inherent in the calculation model and the problem will cause the irrational and inconvergent calculation results.

2) An effective method called massless rigid element (MRE) is presented for solving the problem.

By theoretical and numerical analyses, the proposed method is shown to be an effective and practical method with high computational accuracy. The advantage of the MRE method is that it can be implemented by using the commercially available finite element software such as SAP2000 and be directly applied to practical engineering projects by civil engineers.

This work was supported by the Scientific Research Foundation of Central South University, the National Natural Science Foundation of China (Grant No. 50638010) and the Foundation of Ministry of Education for Innovation Group (Grant No. IRT0518).

1 Hao H. Effects of spatial variation of ground motion on large multiply-supported structures. In: EERC Rep No 89-06, Earthq Eng Res Ctr. Berkeley: University of California, 1989
2 Berrah M, Kausel E. Response spectrum analysis of structures subjected to spatially varying motions. Earthq Eng Struct D, 1992, 21(6): 461–470
3 Yamamura N, Tanaka H. Response analysis of flexible MDF systems for multiple-support seismic excitation. Earthq Eng Struct D, 1990, 19(3): 345–357
4 Hao H. Response of multiply-supported rigid plate to spatially correlated seismic excitations. Earthq Eng Struct D, 1991, 20(9): 821–838
5 Hao H, Xiao N D. Multiple excitation effects on response of symmetric buildings. Eng Struct, 1996, 18(9): 732–740
6 Hao H, Xiao N D. Response of asymmetric structures to multiple ground motions. J Struct Eng, 1995, 121(11): 1557–1564
7 Su L, Dong S L, Kato S. A new average response spectrum method for linear response analysis of structures to spatial earthquake ground motions. Eng Struct, 2006, 28(13): 1835–1842
8 Kahan M, Gibert R. Influence of seismic waves spatial variability on bridges: A sensitivity analysis. Earthq Eng Struct D, 1996, 25(8): 795–814
9 Armen D K, Ansgar N. Response spectrum method for multi-support seismic excitations. Earthq Eng Struct D, 1992, 21(8): 713–740
10 Wang J J. Stochastic model of multi-component multi-support seismic motion and structural response spectrum analysis (in Chinese). Dissertation of Doctor Degree, Harbin: Institute of Engineering Mechanics of State Seismological Bureau, 1992
11 Berrah M, Kausel E. A modal combination rule for spatially varying seismic motions. Earthq Eng Struct D, 1993, 22(9): 791–800
12 Chin H L, B D K. An efficient analysis of structural response for multiple-support seismic excitations. Eng Struct, 1995, 17(1): 15–26
13 Li J, Li J H. A response spectrum method for random vibration analysis of structures under multi-support excitations (in Chinese). Earthq Eng Eng Vib, 2004, 24(3): 21–29
14 Ye J H, Sun J M. Response spectrum method for multi-support seismic excitation (in Chinese). Chinese J Appl Mech, 2007, 24(1): 47–53
15 Wilson E L. Three dimensional static and dynamic analysis of structures: A physical approach with emphasis on earthquake engineering. In: Computers and Structures. California: Inc Berkley, 2002
16 Chopra A K. Dynamics of Structures: Theory and Applications to Earthquake Engineering. 2nd ed. New Jersey: Prentice-Hall Inc, 2000
17 Hughes T. The Finite Element Method——Linear Static and Dynamic Finite Element Analysis. New Jersey: Prentice-Hall Inc, 1987